Calculating splittings between energy levels of different symmetry using path-integral methods

Edit Mátyus[1] and Stuart C. Althorpe[1]

[1]*Department of Chemistry, University of Cambridge, Lensfield Road, Cambridge, CB2 1EW, United Kingdom*

(Dated: 29 February 2016)

Abstract

It is well known that path-integral methods can be used to calculate the energy splitting between the ground and the first excited state. Here we show that this approach can be generalized to give the splitting patterns between all the lowest energy levels from different symmetry blocks that lie below the first-excited totally symmetric state. We demonstrate this property numerically for some two-dimensional models. The approach is likely to be particularly useful for computing rovibrational energy levels and tunnelling splittings in floppy molecules and gas-phase clusters.

I. INTRODUCTION

If a system is symmetric under some operator $\hat{P}$, and if the first excited state is odd with respect to $\hat{P}$, then the splitting ΔE between these levels can be obtained from the ratio,

$$\tanh\left(\frac{1}{2}\Delta E\left[\beta-\bar{\beta}(\boldsymbol{r})\right]\right)=\frac{\rho(\boldsymbol{r},\hat{P}^{-1}\boldsymbol{r};\beta)}{\rho(\boldsymbol{r},\boldsymbol{r};\beta)} \tag{1}$$

where

$$\rho(\boldsymbol{r},\boldsymbol{r}';\beta)=\sum_n \psi_n^*(\boldsymbol{r})\psi_n(\boldsymbol{r}')\mathrm{e}^{-\beta E_n} \tag{2}$$

is the density matrix at inverse temperature β, ψ_n are the system eigenstates (with energy E_n). The ratio in Eq. (1) can be computed using a 'string' variant of Path-integral Monte Carlo or Molecular Dynamics, thus giving a path-integral method which is complementary to diffusion Monte Carlo (DMC) [1–3]. (Note that the splitting of the lowest two energy levels can also be obtained from path-integral methods without relying on the symmetry properties of the system [4–6].)

Such path-integral methods have been used in the past to compute tunnelling splittings in various model symmetric double-well (or analogous) systems [7, 8]. However, as we showed recently in tests on malonaldehyde [9], these methods also appear to be practical for molecular systems, where $\hat{P}$ can be a point-group, permutation-inversion [10] or rotational symmetry operator. Thus Eq. (1) is potentially useful for computing, e.g., tunnelling-splitting patterns in water clusters, where at present only the diffusion Monte Carlo (DMC) method (which suffers from the disadvantage of requiring complete knowledge of the nodal dividing surface) or the projected imaginary-time Monte Carlo method [11, 12] would be applicable. However, before such calculations can be attempted, Eq. (1) needs to be generalized to treat systems with more than one symmetry operation $\hat{P}$.

Here, in Sec. II, we show that it is straightforward to make such a generalization, extending Eq. (1) to give multiple splittings between all the lowest-energy levels of different symmetry that lie below the first-excited totally symmetric state. In Sec. III, we report tests on two-dimensional models to illustrate the feasibility of the approach. Section IV concludes the article.

II. DERIVATION

A. The single-splitting approach

We first summarize the derivation [7–9] of Eq. (1). We define sets of symmetry-related system coordinates $\boldsymbol{r}' = \hat{P}^{-1}\boldsymbol{r} = -\boldsymbol{r}$ such that $\psi_0(\boldsymbol{r}' = -\boldsymbol{r}) = \psi_0(\boldsymbol{r})$ and $\psi_1(\boldsymbol{r}' = -\boldsymbol{r}) = -\psi_1(\boldsymbol{r})$ are respectively the ground and first excited state. We then consider the density matrix elements

$$\rho(\boldsymbol{r}, \boldsymbol{r}; \beta) = |\psi_0(\boldsymbol{r})|^2 \mathrm{e}^{-\beta E_0} + |\psi_1(\boldsymbol{r})|^2 \mathrm{e}^{-\beta E_1} + \ldots \tag{3}$$

$$\begin{aligned} \rho(\boldsymbol{r}, \hat{P}^{-1}\boldsymbol{r}; \beta) &= \psi_0^*(\boldsymbol{r})\psi_0(\hat{P}^{-1}\boldsymbol{r})\mathrm{e}^{-\beta E_0} + \psi_1^*(\boldsymbol{r})\psi_1(\hat{P}^{-1}\boldsymbol{r})\mathrm{e}^{-\beta E_1} + \ldots \\ &= |\psi_0(\boldsymbol{r})|^2 \mathrm{e}^{-\beta E_0} - |\psi_1(\boldsymbol{r})|^2 \mathrm{e}^{-\beta E_1} + \ldots \end{aligned} \tag{4}$$

and for low temperatures (β larger than some $\tilde{\beta}$) we may neglect the contribution of the $n \geq 2$ states. For large β values ($\beta(E_2 - E_0) \gg 1$) we obtain

$$\frac{\rho(\boldsymbol{r}, \hat{P}^{-1}\boldsymbol{r}; \beta)}{\rho(\boldsymbol{r}, \boldsymbol{r}; \beta)} \approx \frac{1 - \mathrm{e}^{-\Delta E(\beta - \bar{\beta}(\boldsymbol{r}))}}{1 + \mathrm{e}^{-\Delta E(\beta - \bar{\beta}(\boldsymbol{r}))}} \tag{5}$$

which gives Eq. (1) with $\bar{\beta}(\boldsymbol{r}) = (2/\Delta E)\ln|\psi_1(\boldsymbol{r})/\psi_0(\boldsymbol{r})|$. In a practical calculation, one computes the ratio Eq. (1) using path-integral importance sampling (Monte Carlo or Molecular Dynamics) at several values of $\beta > \tilde{\beta}$, then fits to a hyperbolic tangent function to extract ΔE. In some cases, linearization of the hyperbolic tangent function is sufficient to yield a good approximation to ΔE.

B. Generalization to multiple splittings

To generalize the single-splitting approach, we write Eq. (4) in matrix form

$$\rho(\boldsymbol{r}, \hat{P}^{-1}\boldsymbol{r}; \beta) = (\psi_0^*(\boldsymbol{r}), \psi_1^*(\boldsymbol{r}), \ldots) \begin{pmatrix} 1 & 0 & 0 & \ldots \\ 0 & -1 & 0 & \ldots \\ 0 & 0 & \vdots & \end{pmatrix} \begin{pmatrix} \psi_0(\boldsymbol{r})\mathrm{e}^{-\beta E_0} \\ \psi_1(\boldsymbol{r})\mathrm{e}^{-\beta E_1} \\ \vdots \end{pmatrix} \tag{6}$$

then note that for the general case we can write down a similar matrix equation

$$
\begin{aligned}
&\rho(\boldsymbol{r}, \hat{P}^{-1}\boldsymbol{r}; \beta) \\
&= \sum_n \sum_{l_n=1}^{d_n} \psi^*_{nl_n}(\boldsymbol{r}) \psi_{nl_n}(\hat{P}^{-1}\boldsymbol{r}) \mathrm{e}^{-\beta E_n} \\
&= \sum_n \sum_{l_n=1}^{d_n} \psi^*_{nl_n}(\boldsymbol{r}) \left(\hat{P} \psi_{nl_n}(\boldsymbol{r}) \right) \mathrm{e}^{-\beta E_n} \\
&= \left(\psi^*_0(\boldsymbol{r}), \boldsymbol{\psi}^\dagger_1(\boldsymbol{r}), \boldsymbol{\psi}^\dagger_2(\boldsymbol{r}), \ldots \right) \underbrace{\begin{pmatrix} \Gamma^{(0)}(\hat{P}) & 0 & 0 & 0 \ \ldots \\ 0 & \boldsymbol{\Gamma}^{(1)}(\hat{P}) & 0 & 0 \ \ldots \\ 0 & 0 & \boldsymbol{\Gamma}^{(2)}(\hat{P}) & 0 \ \ldots \\ 0 & 0 & 0 & \vdots \end{pmatrix}}_{\boldsymbol{K}(\hat{P})} \begin{pmatrix} \psi_0(\boldsymbol{r}) \mathrm{e}^{-\beta E_0} \\ \boldsymbol{\psi}_1(\boldsymbol{r}) \mathrm{e}^{-\beta E_1} \\ \boldsymbol{\psi}_2(\boldsymbol{r}) \mathrm{e}^{-\beta E_2} \\ \vdots \end{pmatrix}
\end{aligned} \tag{7}
$$

where the index l_n labels the degenerate eigenfunctions with the same energy E_n. The degenerate eigenfunctions are collected in the $\boldsymbol{\psi}_n$ vector to highlight the block structure of the matrix $\boldsymbol{K}(\hat{P})$. A symmetry operation, $\hat{P}$, mixes the degenerate eigenfunctions and these functions span the d_n-dimensional λ_n irreducible representation (irrep) of the symmetry group, $\mathbb{G}$. The corresponding irreducible representation matrix for the symmetry operation $\hat{P} \in \mathbb{G}$ is $\boldsymbol{\Gamma}^{(\lambda_n)}(\hat{P}) \in \mathbb{C}^{d_n \times d_n}$, which is the nth diagonal block of $\boldsymbol{K}(\hat{P})$ in Eq. (7). Furthermore, we can assume that the ground state, ψ_0, is non-degenerate and spans the totally symmetric representation with $\Gamma^{(0)}_{\hat{P}} = 1$ for all $\hat{P}$.

We now wish to obtain combinations of density matrix elements that connect individual pairs of levels, such that the splitting between the levels can be calculated using an analogous relation to Eq. (1). For example, to obtain the splitting between the 2nd excited and ground state level (assuming that ψ_0, $\boldsymbol{\psi}_1$, $\boldsymbol{\psi}_2$ have different symmetries and that they are all lower

in energy than the first excited totally symmetric state), we wish to obtain

$$\eta^{(\pm)}_{02,11}(\boldsymbol{r};\beta) = \Big(\psi^*_0(\boldsymbol{r}), \boldsymbol{\psi}^\dagger_1(\boldsymbol{r}), \boldsymbol{\psi}^\dagger_2(\boldsymbol{r}), \ldots\Big) \underbrace{\begin{pmatrix} |\mathbb{G}| & \mathbf{0} & \mathbf{0} & \mathbf{0} & \ldots \\ \mathbf{0} & \mathbf{0} & \mathbf{0} & \mathbf{0} & \ldots \\ \mathbf{0} & \mathbf{0} & \begin{bmatrix} \pm\frac{|\mathbb{G}|}{d_2} & 0 & 0 \\ 0 & 0 & 0 \\ 0 & 0 & 0 \end{bmatrix} & \mathbf{0} & \ldots \\ \mathbf{0} & \mathbf{0} & \mathbf{0} & \vdots & \end{pmatrix}}_{\boldsymbol{X}^{(\pm)}_{02,11}\ (\lambda=2,p=q=1)} \begin{pmatrix} \psi_0(\boldsymbol{r})\mathrm{e}^{-\beta E_0} \\ \boldsymbol{\psi}_1(\boldsymbol{r})\mathrm{e}^{-\beta E_1} \\ \boldsymbol{\psi}_2(\boldsymbol{r})\mathrm{e}^{-\beta E_2} \\ \vdots \end{pmatrix} \tag{8}$$

It is straightforward to derive such equations, using the orthogonality relations for the elements of the irreducible representation matrices. For a finite group $\mathbb{G}$ of order $|\mathbb{G}|$, one uses the great orthogonality theorem

$$\sum_{i=1}^{|\mathbb{G}|} \Big(\boldsymbol{\Gamma}^{(\lambda)}(\hat{P}_i)\Big)^*_{nm} \Big(\boldsymbol{\Gamma}^{(\lambda')}(\hat{P}_i)\Big)_{n'm'} = \delta_{\lambda\lambda'}\delta_{nn'}\delta_{mm'}\frac{|\mathbb{G}|}{d_\lambda}. \tag{9}$$

Clearly this relation holds irrespective of whether we are discussing point-group symmetry or the molecular symmetry (i.e. permutation-inversion) group. For the rotational symmetry group SO(3), we use the analogous relation

$$\int \mathrm{d}\boldsymbol{\Omega}\ D^{(l)}(\boldsymbol{\Omega})^*_{nm} D^{(l')}(\boldsymbol{\Omega})_{n'm'} = \delta_{ll'}\delta_{nn'}\delta_{mm'}\frac{8\pi^2}{2l+1} \tag{10}$$

where we use the Wigner $D^{(l)}(\boldsymbol{\Omega})$ matrix for the irreducible representation matrix of the $\hat{R}_{\boldsymbol{\Omega}}$ rotation operation in the lth irrep and $\mathrm{d}\boldsymbol{\Omega}$ is the volume element including the metric.

For rovibrational applications, the complete symmetry group is the product $\mathbb{G} = \mathrm{SO}(3)\otimes\mathbb{G}_0$, where $\mathbb{G}_0$ is a finite group (which will be either a point-group, for a rigid molecule, or a permutation-inversion group, for a floppy molecule or cluster). Using Eqs. (9) and (10), it is easy to derive that the combination of density matrix elements connecting the (00)th

and the $(l\lambda)$th irreps is

$$\eta^{(\pm)}_{(00)(l\lambda),pq}(\boldsymbol{r};\beta) = \int \mathrm{d}\boldsymbol{\Omega} \sum_{i=1}^{|\mathbb{G}_0|} \left[1 \pm D^{(l)}_{p_l q_l}(\boldsymbol{\Omega})^* \left(\boldsymbol{\Gamma}^{(\lambda)}(\hat{P}_i) \right)^*_{p_\lambda q_\lambda} \right] \rho(\boldsymbol{r}, (\hat{R}_{\boldsymbol{\Omega}} \hat{P}_i)^{-1} \boldsymbol{r};\beta) \tag{11}$$

where we also used the property that the totally symmetric irrep is represented by unity. For other symmetry groups a similar expression can be obtained by performing the summation or integration for the corresponding irreducible matrix elements of the group operations (further examples are provided in Sec. III).

For large enough β values the population of the excited states of the (00)th totally symmetric and of the $(l\lambda)$th irrep is negligible (see Fig. 1), and we are left with the leading terms:

$$\eta^{(\pm)}_{(00)(l\lambda),pp}(\boldsymbol{r};\beta) \approx |\mathbb{G}||\psi_{00}(\boldsymbol{r})|^2 \mathrm{e}^{-\beta E_{00}} \pm \frac{|\mathbb{G}|}{d_{l\lambda}} \cdot |\psi_{l\lambda,p}(\boldsymbol{r})|^2 \mathrm{e}^{-\beta E_{l\lambda}} \qquad (\beta > \tilde{\beta}) \tag{12}$$

which, similarly to the double-well case, Eq. (1), can be used to obtain the expression

$$\begin{aligned} \frac{\eta^{(-)}_{(00)(l\lambda),pp}(\boldsymbol{r};\beta)}{\eta^{(+)}_{(00)(l\lambda),pp}(\boldsymbol{r};\beta)} &= \frac{|\psi_{00}(\boldsymbol{r})|^2 \mathrm{e}^{-\beta E_{00}} - \frac{1}{d_{l\lambda}} |\psi_{l\lambda,p}(\boldsymbol{r})|^2 \mathrm{e}^{-\beta E_{l\lambda}}}{|\psi_{00}(\boldsymbol{r})|^2 \mathrm{e}^{-\beta E_{00}} + \frac{1}{d_{l\lambda}} |\psi_{l\lambda,p}(\boldsymbol{r})|^2 \mathrm{e}^{-\beta E_{l\lambda}}} \\ &= \tanh\left(\frac{1}{2} \Delta E_{00,l\lambda} \left[\beta - \bar{\beta}_{00,l\lambda}(\boldsymbol{r}) \right] \right) \end{aligned} \tag{13}$$

for the energy-level difference

$$\Delta E_{00,l\lambda} = E_{l\lambda} - E_{00} \tag{14}$$

and $\bar{\beta}_{00,l\lambda}(\boldsymbol{r}) = (2/\Delta E_{00,l\lambda}) \ln |\psi_{l\lambda}(\boldsymbol{r})/(\sqrt{d_{l\lambda}}\psi_{00}(\boldsymbol{r}))|$. Thus, the relation between the energy levels (measured from the totally symmetric ground state) and the density matrix elements

for the example of $\mathbb{G} = \mathrm{SO}(3) \otimes \mathbb{G}_0$ is

$$\begin{aligned}
&\tanh\left(\frac{1}{2}\Delta E_{00,l\lambda}\left[\beta - \bar{\beta}_{00,l\lambda}(\boldsymbol{r})\right]\right) \\
&= \frac{\eta^{(-)}_{(00)(l\lambda),pp}(\boldsymbol{r};\beta)}{\eta^{(+)}_{(00)(l\lambda),pp}(\boldsymbol{r};\beta)} \\
&= \frac{\int \mathrm{d}\boldsymbol{\Omega} \sum_{i=1}^{|\mathbb{G}_0|} \left(1 - D^{(l)}(\boldsymbol{\Omega})^*_{p_l p_l} \left(\boldsymbol{\Gamma}^{(\lambda)}(\hat{P}_i)\right)^*_{p_\lambda p_\lambda}\right) \rho(\boldsymbol{r}, (\hat{R}_{\boldsymbol{\Omega}}\hat{P}_i)^{-1}\boldsymbol{r};\beta)}{\int \mathrm{d}\boldsymbol{\Omega} \sum_{i=1}^{|\mathbb{G}_0|} \left(1 + D^{(l)}(\boldsymbol{\Omega})^*_{p_l p_l} \left(\boldsymbol{\Gamma}^{(\lambda)}(\hat{P}_i)\right)^*_{p_\lambda p_\lambda}\right) \rho(\boldsymbol{r}, (\hat{R}_{\boldsymbol{\Omega}}\hat{P}_i)^{-1}\boldsymbol{r};\beta)} \\
&\qquad\qquad (\beta > \tilde{\beta}).
\end{aligned} \tag{15}$$

Exploiting the isotropy of space (for an isolated molecule or cluster) simplifies the triple integral of the rotation angles in Eq. (15) to

$$\begin{aligned}
&\tanh\left(\frac{1}{2}\Delta E_{00,l\lambda}\left[\beta - \bar{\beta}_{00,l\lambda}(\boldsymbol{r})\right]\right) \\
&= \frac{\int_0^\pi \mathrm{d}(\cos\theta) \sum_{i=1}^{|\mathbb{G}_0|} \left(1 - P_l(\cos\theta) \left(\boldsymbol{\Gamma}^{(\lambda)}(\hat{P}_i)\right)^*_{p_\lambda p_\lambda}\right) \rho(\boldsymbol{r}, (\hat{R}_{\boldsymbol{n},\theta}\hat{P}_i)^{-1}\boldsymbol{r};\beta)}{\int_0^\pi \mathrm{d}(\cos\theta) \sum_{i=1}^{|\mathbb{G}_0|} \left(1 + P_l(\cos\theta) \left(\boldsymbol{\Gamma}^{(\lambda)}(\hat{P}_i)\right)^*_{p_\lambda p_\lambda}\right) \rho(\boldsymbol{r}, (\hat{R}_{\boldsymbol{n},\theta}\hat{P}_i)^{-1}\boldsymbol{r};\beta)} \\
&\qquad\qquad (\beta > \tilde{\beta})
\end{aligned} \tag{16}$$

where $P_l(\cos\theta)$ is the lth Legendre polynomial and $\boldsymbol{n}$ defines some rotation axis.

This equation gives an expression for the energy difference, $\Delta E_{00,l\lambda}$, of the lowest-lying energy level of the λth irrep with rotational quantum number $J = l$ and the ground-state energy with $J = 0$, in terms of the low-temperature behavior of the quantum thermal density matrix elements connecting symmetry-related structures. Using this symmetrization equation the lowest-energy level of (in principle) any irrep can be accessed which is below the first excited state of the totally symmetric irrep with $J = 0$ (see Fig. 1). Since we chose the totally symmetric irrep with $J = 0$ as a "reference state", it can be shown that the integration and linear combination coefficients of the symmetrization equations, Eq. (11), are all non-negative and hence, non-oscillatory. (This observation is true in general for any symmetry group as long as we choose the lowest energy level of the totally symmetric irrep as the reference state in the equations.) For multi-dimensional irreps there are infinitely many

such matrices (related by unitary transformation), but any set of the irreducible matrices can be selected, because $\rho(\boldsymbol{a},\boldsymbol{b};\hat{P})$ is representation free in this sense.

To evaluate $\eta^{(-)}_{(00)(l\lambda),pp}(\boldsymbol{r};\beta)/\eta^{(+)}_{(00)(l\lambda),pp}(\boldsymbol{r};\beta)$ by path-integral importance sampling, one divides top and bottom of Eqs. (15)–(16) by the density matrix element $\rho(\boldsymbol{r},\boldsymbol{r};\beta)$. (In the special case of a single splitting, the equations simplify to Eq. (1).) The one-dimensional integral in θ can be evaluated numerically by quadrature.

III. NUMERICAL APPLICATIONS

We tested the feasibility of the approach by applying it to the set of two-dimensional models illustrated in Fig. 2. These systems were chosen because they illustrate the most likely applications of the approach: multi-well tunnelling (Figs. 2a–c), fluxional systems (Fig. 2e), and rotational levels (Fig. 2d). The density matrix ratios connecting symmetry-related structures, $\rho(\boldsymbol{r},\hat{P}_i^{-1}\boldsymbol{r};\beta)/\rho(\boldsymbol{r},\boldsymbol{r};\beta)$, were calculated using the PIMD approach of Ref. [9] and the the symmetry analyses were carried out within the appropriate C_n and SO(2) groups. Further details of the calculations are provided in the following subsections.

A. Computational details: Hamiltonian and potential energy surface

We carried out example calculations (see Fig. 2 and Fig. S1 of the Supplemental Material [13]) using the Hamiltonian (in atomic units)

$$\hat{H}_n = -\frac{1}{2}\left(\frac{\partial^2}{\partial x^2}+\frac{\partial^2}{\partial y^2}\right)+V_n(x,y) \tag{17}$$

with the potential energy surfaces

$$V_n(x,y) = -\frac{1}{2}\sum_{k=0}^{n-1}\left(\mathrm{e}^{-a\left[(x-x_k)^2-(y-y_k)^2\right]}+\mathrm{e}^{-b\left[(x-x_k)^2-(y-y_k)^2\right]}\right) \tag{18}$$
$$\text{with}\quad (x_k,y_k)=\rho_0\left(\cos\frac{2\pi k}{n},\sin\frac{2\pi k}{n}\right),\ k=0,1,\ldots,n-1$$

of D_n ($n=2,3,\ldots,6$) point group symmetry. In Eq. (18) we used $\rho_0=3$, $a=2$, and $b=0.2$ to model multi-well tunneling, $V_n(x,y)$ ($n=2,3,\ldots,6$), and $\rho_0=1$ and $a=b=0.5$ to obtain a barrierless potential energy surface of three-fold dihedral symmetry, $V_3'(x,y)$ to

model a fluxional system. The potential energy surface of O(2) point-group symmetry was

$$V_\infty(x,y) = -\frac{1}{2}\left(\mathrm{e}^{-2(r-3)^2} + \mathrm{e}^{-0.2(r-3)^2}\right) \quad \text{with} \quad r = \sqrt{x^2+y^2}. \tag{19}$$

For the symmetry analysis we used the corresponding cyclic subgroups, C_n ($n = 2, 3, \ldots, 6$) and SO(2). A similar, slightly more involved, analysis can be carried out for the lowest energy levels of the irreps of D_n ($n = 2, 3, \ldots, 6$) and O(2). As it is highlighted in Fig. 1 only those energy levels can be obtained within this symmetrization approach which are lower in energy than the first excited state of the totally symmetric irrep (and are below the dissociation limit). For the present parameterization of the example systems the cyclic subgroups and SO(2) deliver all accessible information.

B. Computational details: symmetrization in $\mathbf{C}_n$

For the mth irrep of a system with $\mathbb{G} = \mathrm{C}_n$ symmetry the equivalent of Eq. (11) is

$$\eta^{(\mp)}_{0m,11}(\boldsymbol{r}_0;\beta) = \sum_{k=0}^{n-1}\left[1 \mp \left(\Gamma^{(m)}_{11}(\hat{R}_k)\right)^*\right]\rho(\boldsymbol{r}_0, \hat{R}_k^{-1}\boldsymbol{r}_0;\beta) \tag{20}$$

which connects the 0th ground state and the lowest energy level in the mth irrep of C_n. $\hat{R}_k$ is a rotation operator about the n-fold rotation axis by an angle of $2\pi k/n$. The symmetrization is carried out using the (1,1) element of the irreducible representation matrix of $\hat{R}_k$ in the mth irrep, denoted by $\Gamma^{(m)}_{11}(\hat{R}_k)$. In this work, we use the basis vectors, $\varphi \in [0, 2\pi)$,

$$\begin{pmatrix} \chi_{-m}(\varphi) \\ \chi_m(\varphi) \end{pmatrix} = \frac{1}{\sqrt{2\pi}}\begin{pmatrix} \mathrm{e}^{-\mathrm{i}m\varphi} \\ \mathrm{e}^{\mathrm{i}m\varphi} \end{pmatrix} \tag{21}$$

to construct the 2-dimensional irreducible representation matrices for the rotation operators, which give rise to

$$\Gamma^{(m)}_{11}(\hat{R}_k) = \mathrm{e}^{\mathrm{i}m\frac{2\pi k}{n}} \quad \text{for} \quad m = 1, \ldots, \lfloor n/2 \rfloor - 1. \tag{22}$$

For even n the function $\chi_{n/2}(\varphi) = \mathrm{e}^{\mathrm{i}n/2\varphi}/\sqrt{2\pi}$ spans a one-dimensional irrep with $\Gamma_{11}^{(m)}(\hat{R}_k) = (-1)^k$ character. Thereby, the explicit form of Eq. (20) is

$$\eta_{0m,11}^{(\mp)}(\boldsymbol{r}_0;\beta) = \sum_{k=0}^{n-1} c_k^{(m,\mp)} \rho(\boldsymbol{r}_0, \hat{R}_k^{-1}\boldsymbol{r}_0;\beta) \quad \text{with} \quad c_k^{(m,\mp)} = 1 \mp \mathrm{e}^{-\mathrm{i}m\frac{2\pi k}{n}} \qquad (23)$$

$$\text{for} \quad m = 0, 1, \ldots, \lfloor n/2 \rfloor.$$

The elementary amplitudes, $\rho(\boldsymbol{r}_0, \hat{R}_k^{-1}\boldsymbol{r}_0;\beta)$, used to form the symmetrized amplitude, $\eta_{0m,11}^{(\mp)}(\boldsymbol{r}_0;\beta)$, are visualized in Fig. 3 for the example of the C_5 group.

C. Computational details: symmetrization in SO(2)

For the mth irrep of a system with $\mathbb{G} = \mathrm{SO}(2)$ symmetry the equivalent of Eq. (11) takes the form

$$\eta_{0m,11}^{(\mp)}(\boldsymbol{r}_0;\beta) = \int_0^{2\pi} \mathrm{d}\varphi \left[1 \mp \left(\Gamma_{11}^{(m)}(\hat{R}_\varphi)\right)^*\right] \rho(\boldsymbol{r}_0, \hat{R}_\varphi^{-1}\boldsymbol{r}_0;\beta) \qquad (24)$$

$$= \int_0^{2\pi} \mathrm{d}\varphi \left[1 \mp \mathrm{e}^{-\mathrm{i}m\varphi}\right] \rho(\boldsymbol{r}_0, \hat{R}_\varphi^{-1}\boldsymbol{r}_0;\beta) \qquad (25)$$

$$\approx \sum_{i=0}^{N-1} c_i^{(m,\mp)} \rho(\boldsymbol{r}_0, \hat{R}_{\varphi_i}^{-1}\boldsymbol{r}_0;\beta) \quad \text{with} \quad c_i^{(m,\mp)} = w_i \left[1 \mp \mathrm{e}^{-\mathrm{i}m\varphi_i}\right]. \qquad (26)$$

$\hat{R}_\varphi$ is the operator of a rotation by angle φ about the rotation axis. To construct the irreducible representation matrices we can use the basis vectors of Eq. (21) with $m = 1, 2, \ldots$ In the practical calculations the integral for φ is approximated numerically over a grid of N points, Eq. (26). The minimum number of grid points increases with m. For example, the energy splitting ΔE_{0m} with $m = 1$ can be obtained already with $N = 2$ points.

D. Computational details: path-integral molecular dynamics simulation to calculate the density-matrix ratios

We write the symmetrized density matrix ratio as

$$\begin{aligned}\frac{\eta^{(-)}_{0m,11}(\boldsymbol{r}_0;\beta)}{\eta^{(+)}_{0m,11}(\boldsymbol{r}_0;\beta)} &= \frac{\sum_{k=0}^{n-1} c_k^{(-)} \rho(\boldsymbol{r_0}, \hat{R}_k^{-1}\boldsymbol{r}_0;\beta)}{\sum_{k=0}^{n-1} c_k^{(+)} \rho(\boldsymbol{r_0}, \hat{R}_k^{-1}\boldsymbol{r}_0;\beta)} \\ &= \frac{\sum_{k=0}^{n-1} c_k^{(-)} \rho(\boldsymbol{r_0}, \hat{R}_k^{-1}\boldsymbol{r}_0;\beta)/\rho(\boldsymbol{r}_0,\boldsymbol{r}_0;\beta)}{\sum_{k=0}^{n-1} c_k^{(+)} \rho(\boldsymbol{r_0}, \hat{R}_k^{-1}\boldsymbol{r}_0;\beta)/\rho(\boldsymbol{r}_0,\boldsymbol{r}_0;\beta)}\end{aligned} \tag{27}$$

and calculate $\rho(\boldsymbol{r_0}, \hat{R}_k^{-1}\boldsymbol{r}_0,\beta)/\rho(\boldsymbol{r}_0,\boldsymbol{r}_0;\beta)$ with PIMD using the implementation of Ref. [9]. For the C_n finite groups $n = |\mathbb{G}|$ and for SO(2) $n = N$ is the number of integration points in Eq. (26). In this paragraph, we summarize the method of Ref. [9] and specify the simulation parameters. Using the classical isomorphism of the path-integral formalism, $\rho(\boldsymbol{a},\boldsymbol{b};\beta)$ is represented with a classical phase space integral for a hypothetical linear polymer with its two end points fixed at $\boldsymbol{a}$ and at $\boldsymbol{b}$. $\rho(\boldsymbol{r_0}, \hat{R}_k^{-1}\boldsymbol{r}_0;\beta)/\rho(\boldsymbol{r}_0,\boldsymbol{r}_0;\beta)$ is calculated from the free-energy difference (obtained by thermodynamic integration) of an open linear polymer with end points fixed at $\boldsymbol{r}_0$ and at $\hat{R}_k^{-1}\boldsymbol{r}_0$ and a closed linear polymer with both end points fixed at $\boldsymbol{r}_0$. In the present work results are shown for $\boldsymbol{r}_0^{\mathrm{T}} = (3, 0)$. The number of beads, $M + 1$, the total simulation time, $t_{\max}$ (in atomic units), and the number of Gauss–Legendre quadrature points, N_ξ, (used in the thermodynamic integration) are given as $(M, t_{\max}, N_\xi)$ in each row of the Tables S1–S7 of the Supplemental Material. Collection of data started after an initial equilibration of 10–30 % of $t_{\max}$. For the other simulation parameters, we used a time step of 10^{-2} (in atomic units), normal-mode scaling (each normal mode of the linear polymer scaled to $\tilde{\Omega} = 1$), and a massive Andersen thermostat with a collision frequency of 1000.

E. Computational details: fitting the energy splittings

To obtain the energy splitting, ΔE_{0m}, we fit the function

$$\frac{\eta^{(-)}_{0m,11}(\boldsymbol{r}_0;\beta)}{\eta^{(+)}_{0m,11}(\boldsymbol{r}_0;\beta)} = \tanh\left(\frac{1}{2}\Delta E_{0m}\left[\beta - \bar{\beta}_{0m}(\boldsymbol{r}_0)\right]\right). \tag{28}$$

to a dataset $\left(\beta_i, \eta^{(-)}_{0m,11}(\boldsymbol{r}_0;\beta_i)/\eta^{(+)}_{0m,11}(\boldsymbol{r}_0;\beta_i)\right)$ $(i = 1, 2, \ldots, N_{\mathrm{data}})$. $\bar{\beta}_{0m}(\boldsymbol{r}_0)$ is also obtained and carries information about the relative amplitude of the wave functions. An accurate ΔE_{0m} value is obtained if β is large enough to depopulate excited states in the 0th (totally symmetric) and in the mth irreps (see also Fig. 1). In practice, an optimal β range is determined (in a series of calculations), in which the excited states are sufficiently depopulated but β is as low as possible to keep the cost of the simulations low and to have sufficient populations in the desired states. In the present examples $\tilde{\beta} \approx 5$.

F. Discussion

The PIMD energy-level splittings (Fig. 2) are in excellent agreement with the variational results obtained with the program of Ref. [14]. An important question is whether the symmetrization equations, Eqs. (11), (16) (and Eqs. (20), (26)) lead to additional computational costs on top of what would be required in a standard application of Eq. (1) (to compute a single splitting). Clearly, the number of ratios $\rho(\boldsymbol{r}, \hat{P}_i^{-1}\boldsymbol{r};\beta)/\rho(\boldsymbol{r},\boldsymbol{r};\beta)$ scales as the number of operations $\hat{P}$ and hence with the number of energy-level splittings calculated. Note that if the molecular symmetry group is very large, it is not necessary to draw $\hat{P}$ from the complete permutation-inversion group (which grows factorially with the number of identical particles); one can draw $\hat{P}$ from a subgroup (for example, the molecular symmetry group), containing just a few operations. For each $\hat{P}$, the evaluation of $\rho(\boldsymbol{r}, \hat{P}_i^{-1}\boldsymbol{r};\beta)/\rho(\boldsymbol{r},\boldsymbol{r};\beta)$ takes up a comparable amount of computational effort to what is required to calculate the single ratio in Eq. (1). Hence, the overall cost of the approach scales as the number of potential energy gradient evaluations, which usually grows approximately linearly with system size. As with the application of Eq. (1) [9], the cost also increases if an operator $\hat{P}_n$ pushes the system through a high barrier, and increases with the value of $\tilde{\beta}$ needed to eliminate contributions from excited states (within the selected irrep).

IV. SUMMARY AND OUTLOOK

We have demonstrated that it is feasible to use path-integral methods to calculate energy splittings between all lowest energy levels of different irreducible symmetry that lie below the first-excited totally symmetric state. The approach uses space-fixed Cartesian coordinates,

and does not require knowledge of the nodal dividing surface, since the symmetry operations need to be applied to just one Cartesian structure.

For each symmetry operation, the cost of such a calculation is comparable to that of applying Eq. (1). Recent work [9] has shown that Eq. (1) can be used to compute the tunnelling splitting of malonaldehyde, and that with further development it is likely to be able to treat larger systems. The approach developed here should thus be similarly applicable, and should complement the DMC method [1–3] (which requires knowledge of the nodal dividing surface, except for the ground state). Systems to which it is likely to be applicable (which satisfy the essential condition of having levels below the first-excited totally symmetric state) include the splitting patterns of water clusters (where it would provide an exact generalization of multi-well instanton theory [15–19] and related semiclassical methods [20]) and the rovibrational levels of fluxional molecules.

Acknowledgment

EM and SCA acknowledge funding from the UK Engineering and Physical Sciences Research Council.

[1] J. B. Anderson, J. Chem. Phys. **63**, 1499 (1975).

[2] M. Quack and M. A. Suhm, Chem. Phys. Lett. **234**, 71 (1995).

[3] A. B. McCoy, Int. Rev. Phys. Chem. **25**, 77 (2006).

[4] A. Kuki and P. G. Wolynes, Science **236**, 1647 (1987).

[5] C. Alexandrou and J. W. Negele, Phys. Rev. C **37**, 1513 (1988).

[6] M. Marchi and D. Chandler, J. Chem. Phys. **95**, 889 (1991).

[7] D. M. Ceperley and G. Jacucci, Phys. Rev. Lett. **58**, 1648 (1987).

[8] D. M. Ceperley, Rev. Mod. Phys. **67**, 279 (1995).

[9] E. Mátyus, D. J. Wales, and S. C. Althorpe, submitted to J. Chem. Phys. (2016).

[10] P. R. Bunker and P. Jensen, *Molecular Symmetry and Spectroscopy, 2nd Edition* (NRC Research Press, Ottawa, 1998).

[11] D. Blume, M. Lewerenz, and K. B. Whaley, J. Chem. Phys. **107**, 9067 (1997).

[12] D. Blume, M. Lewerenz, P. Niyaz, and K. B. Whaley, Phys. Rev. E **55**, 3664 (1997).

[13] The Supplemental Material at [URL will be inserted by AIP] provides further details about the path-integral molecular dynamics simulations.

[14] E. Mátyus, G. Czakó, and A. G. Császár, J. Chem. Phys. **130**, 134112 (2009).

[15] W. H. Miller, J. Chem. Phys. **62**, 1899 (1975).

[16] J. O. Richardson and S. C. Althorpe, J. Chem. Phys. **134**, 054109 (2011).

[17] J. O. Richardson, S. C. Althorpe, and D. J. Wales, J. Chem. Phys. **135**, 124109 (2011).

[18] J. O. Richardson, D. J. Wales, S. C. Althorpe, R. P. McLaughlin, M. R. Viant, O. Shih, and R. J. Saykally, J. Phys. Chem. A **117**, 6960 (2013).

[19] J. O. Richardson, C. Pérez, S. Lobsiger, A. A. Reid, B. Temelso, G. C. Shields, Z. Kisiel, D. J. Wales, B. H. Pate, and S. C. Althorpe, Science (in press) (2016).

[20] N. Makri and W. H. Miller, J. Chem. Phys. **91**, 4026 (1989).

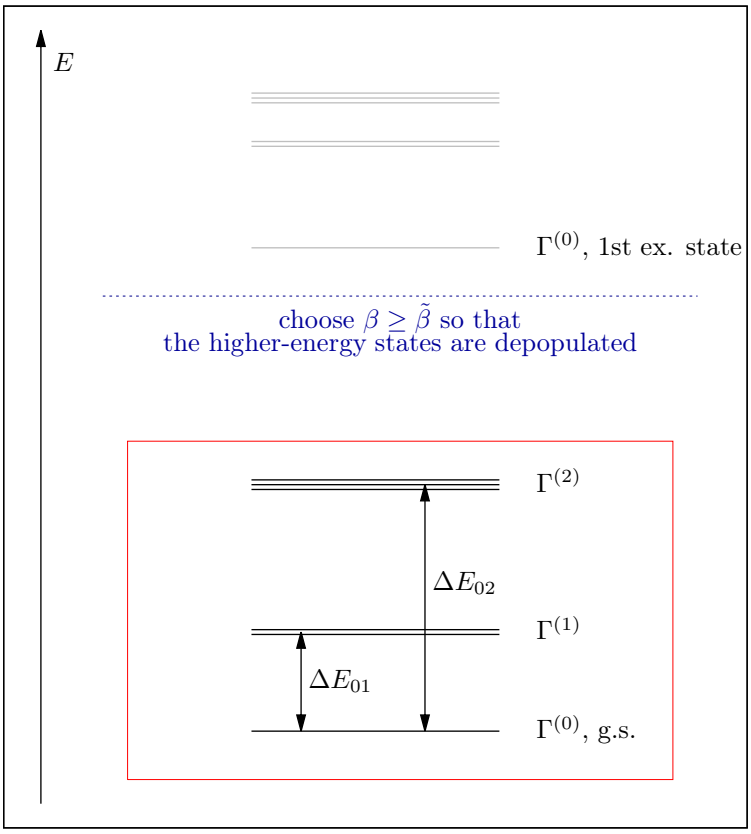

FIG. 1: Schematic showing the energy splittings which can be obtained from the proposed path-integral method. (The degenerate energy levels have been artificially split to make the figure self-explanatory; "g.s." and "ex. state" denote the ground and excited state.)

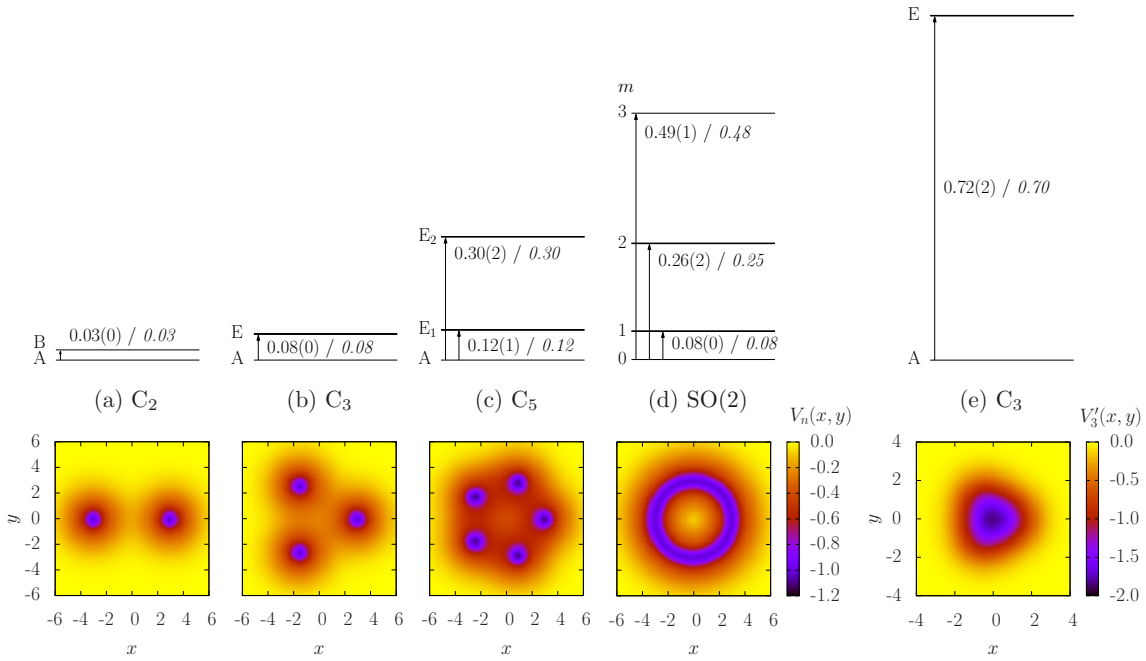

FIG. 2: Lowest energy levels of different irreducible symmetry calculated using path-integral molecular dynamics (PIMD), for a variety of two-dimensional models with n-fold dihedral symmetry (shown at bottom). Also shown are the exact results from variational calculations (italics). The corresponding C_n or SO(2) subgroups were used to extract the energy-level splittings, using the procedure of Sec. II. The functional forms of the potential energy surfaces and all other details of the calculations are provided in Sec. III. Atomic units are used throughout this work.

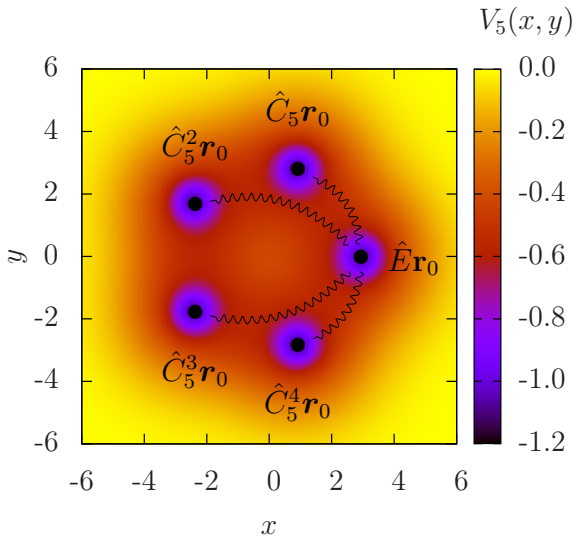

FIG. 3: Visualization of using the C_5 symmetry group and PIMD simulations on the $V_5(x,y)$ potential energy surface to calculate the splitting of the lowest energy levels of different symmetry.